Millimeter-Wave Ferromagnetic Resonance of a Saturated Magnetic Transmission Line

Muhammad Shamaas[1], Muhammad Asghar Saqib[2], Syed Abdul Rahman Kashif[3] and Syed Shah Irfan Hussain[4]

[1, 2, 3, 4]Department of Electrical Engineering, University of Engineering and Technology, Lahore 54890, Pakistan

[1]2018msee004@student.uet.edu.pk, [2]saqib@uet.edu.pk, [3]abdulrahaman@uet.edu.pk, [4]ssirfanhussain@uet.edu.pk,

Abstract –*Saturated ferromagnets exhibit microwave and millimeter wave absorption because they consist of nano-magnetic harmonic oscillators. The absorption frequency and line width are dictated by the strength and range of interactions between the magnetic dipoles. The forced orientation of magnetic dipoles along the magnetic bias results in Zeeman splitting in the energy levels. The incoming electromagnetic wave can excite dipoles to transition between these energy levels. In order to investigate the effects of input frequency and Gilbert damping constant on the electromagnetic properties, a magnetic transmission line model is presented for a saturated ferromagnet. The enhanced power loss during ferromagnetic resonance is contributed to the strong spike of longitudinal magnetic admittance and transverse magnetic impedance.*

Keywords: Magnetic transmission line, longitudinal magnetic admittance, transverse magnetic impedance, ferromagnetic resonance line width

I. INTRODUCTION

Gyromagnetic materials are widely used in high-frequency applications such as microwave devices and radar communication because of their directional and non-reciprocal properties. These materials exhibit ferromagnetic resonance in the micro and mm-wave region under the influence of external magnetostatic bias fields. During ferromagnetic resonance their affinity for magnetic flux increases greatly enabling them to conduct magnetic information efficiently. The heightened permeability and resistivity is extremely useful for microwave devices, isolators, circulators and absorbers [1].

Ferromagnetic materials change their electromagnetic properties when a magnetic bias field is applied [2]. The bias field produces Zeeman splitting in energy levels and the saturated magnetic dipoles can transition between the energy levels by absorbing microwave or millimeter wave electromagnetic fields [3]. The non-linear and anisotropic nature of magnetized ferrites can be modeled using a non-diagonal magnetic susceptibility tensor. Specialized electron spin resonance spectrometer and network analyzer are required to estimate the dispersion characteristics of the susceptibility tensor elements. The precessional magnetization dynamics can be experimentally observed using resonant cavity, strip-line transducer or shorted waveguide technique [4]. The power absorption and ferromagnetic resonance spectrum line width of a gyromagnetic ferrite is highly sensitive to the frequency dependence of the susceptibility tensor elements. The magnetic properties of microwave ferrites vary widely with chemical composition, crystal structure and bias field [5]. The nano-magnetic exchange interactions and dipole-dipole interactions dictate the excitation of spin waves in the magnetized medium [6]. Realistic system level models for the analysis of ferromagnetic materials must account for the characteristic information delay, distortion and attenuation.

Ferromagnetic resonance can be analyzed experimentally using a quasi-optical spectrometer or a vector network analyzer. In reference [3], a high frequency spectrometer was used to determine the effect of complex dielectric permittivity and magnetic permeability on the transmission and reflection coefficients during millimeter wave ferromagnetic resonance; with special emphasis on the effect of magnetic domain size and crystal structure on the ferromagnetic resonance frequency. In reference [6], a magneto-optical method was used to detect the effect of crystal structure, frequency and direct current (DC) magnetic bias on the ferromagnetic resonance spectrum peak and line width. A vector network analyzer was used to obtain multi-mode ferromagnetic spectrum for a ferrite loaded coplanar waveguide in reference [7]. The scattering parameters are directly affected by the dispersion of magnetic permeability, structural dimensions, formation of standing waves

and parasitic effects [8]. A mixture of standing wave and magnetostatic modes were excited depending on the applied magnetic bias and structural dimensions, which translated into unwanted resonances in the output spectrum [9]. These methods are highly accurate for detecting ferromagnetic resonance, but they offer very limited information about the magnetized ferrite and the individual resonance modes.

The electric transmission line model is commonly used to explain non-reciprocal properties of magnetized ferromagnets [10]. In reference [2], frequency dependent behaviour of complex permeability and permittivity of a ferromagnetic transmission line was calculated using an impedance analyzer. The measured intrinsic impedance and propagation constant were used to determine the transmission line impedance and admittance. Although the results were only applicable to the transverse electromagnetic (TEM) wave propagation; this is a very powerful technique to study electromagnetic characteristics of a magnetized ferrite. In reference [5], the magneto-impedance of saturated ferrites during ferromagnetic resonance was analyzed for different crystal structures. The resonance intensity and line width are dependent on the dominant magnetization process [5], Gilbert damping constant [11] and magnetic permeability [12]. Shorted microstrip transmission line perturbation technique was used to calculate the complex permeability during ferromagnetic resonance of a coplanar waveguide in reference [8]. Transmission line methods are suitable for the study of magnetized ferrites because individual wave modes can be studied and the electromagnetic properties of the transmission medium can be accurately modeled using an equivalent core impedance.

The transcendental equations for propagation of electrodynamic fields in gyromagnetic media do not have a close form solution so they must be solved via electromagnetic simulations [13]. The propagation of extremely high frequency (EHF) signals in dispersive, anisotropic, conductive ferromagnetic cores has been widely studied using finite difference simulations [4]. In reference [10], propagation of high frequency electromagnetic fields in a waveguide filled with anisotropic, magnetized ferrite was analyzed. The effect of frequency on the attenuation constant and phase constant was studied using finite difference frequency domain (FDFD) simulations and analytical results. However, the results were only applicable to two-dimensional ferrites with a fixed damping ratio and DC magnetic bias. The effect of complex permeability and permittivity on the transmission line impedance and propagation constant was studied using finite difference time domain (FDTD) simulations in reference [4]. During millimeter wave ferromagnetic resonance, the frequency dependent complex susceptibility tensor determines the steady state amplitude, phase and ellipticity of the resultant electromagnetic wave [9]. Finite difference micro-magnetic simulations can accurately model the precessional magnetization dynamics, and the results are comparable to analytical results. They are very useful for studying individual resonance modes while excluding the formation of standing waves due to unwanted magnetic pinning.

Unlike electric transmission lines, these magnetic circuits are not designed to conduct electric charge upon application of electromotive force. As shown in Figure 1, the transverse electric field lines are closed, encircling the magnetic wire; while the transverse magnetic field lines are open, starting at the magnetic wire. The experimental results must be translated into an electromagnetic transmission line system level design which can explain the flow of magnetic flux due to the application of magnetomotive force. Such a model is presented in reference [14]. For magnetic transmission lines, transverse magnetic impedance and the longitudinal magnetic admittance determine the propagation constants for the wave modes. The magnetic transmission line exhibited the behaviour of a high-pass filter; and simulations showed that they exhibit super-luminal phase velocity and almost zero attenuation dispersion in the microwave-frequency range [15].

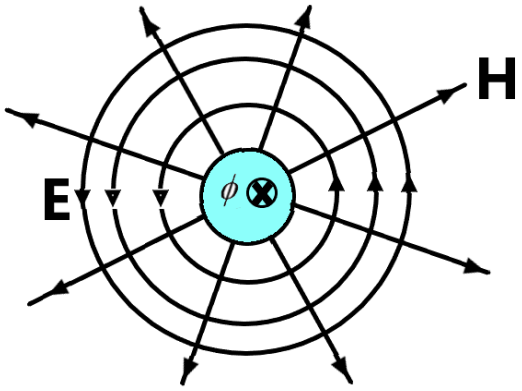

Figure 1: Transverse field lines for a magnetic transmission line.

The magnetic transmission line model explains the flow of magnetic flux in ferromagnetic materials as the effective magnetic charge. It provides a system level circuit for relating magnetomotive force to the applied magnetic flux rate. Analogous to the scalar electric potential in electric transmission lines, scalar magnetic

potential V_{ab} is defined as the line integral of magnetic field intensity vector $\boldsymbol{H}$ from point a to b:

$$V_{ab} = \int_a^b \boldsymbol{H}.dl \tag{1}$$

The magnetic displacement current I_m is defined as the rate of change of magnetic flux Φ_m:

$$I_m = \frac{d}{dt}\oint \boldsymbol{B}.ds = \frac{d\Phi_m}{dt} \tag{2}$$

where $\boldsymbol{B}$ is the magnetic flux density vector.

The magnetic transmission line equivalent circuit is shown in Figure 2. The magnetic transmission line equations [14] can be written as:

$$\frac{d}{dz}\begin{bmatrix} I_m \\ V_m \end{bmatrix} = \begin{bmatrix} 0 & 0 \\ -G_L & 0 \end{bmatrix}\begin{bmatrix} I_m \\ V_m \end{bmatrix} + \begin{bmatrix} 0 & -L_T \\ -C_L & 0 \end{bmatrix}\frac{d}{dt}\begin{bmatrix} I_m \\ V_m \end{bmatrix} \tag{3}$$

where the per unit length transverse magnetic inductance L_T represents a magnetic energy storage element storing magnetic flux; the per unit length longitudinal capacitance C_L represents an electric energy storage element resulting from the dielectric nature of the ferromagnet; and the per unit length magnetic conductance G_L dissipates energy due to hysteresis, eddy currents, skin effect, proximity effect, magnetoresistance and other residual losses [15]. The characteristic impedance η and propagation constant γ are calculated by the following relations:

$$\eta(j\omega) = \frac{I_m(j\omega)}{V_m(j\omega)} = \sqrt{\frac{Z_T(j\omega)}{Y_L(j\omega)}} \tag{4}$$

$$\gamma(j\omega) = \sqrt{Z_T(j\omega)Y_L(j\omega)} \tag{5}$$

where $Z_T(j\omega) = j\omega L_T$ is the transverse magnetic impedance and $Y_L(j\omega) = G_L + j\omega C_L$ is the longitudinal magnetic admittance [14].

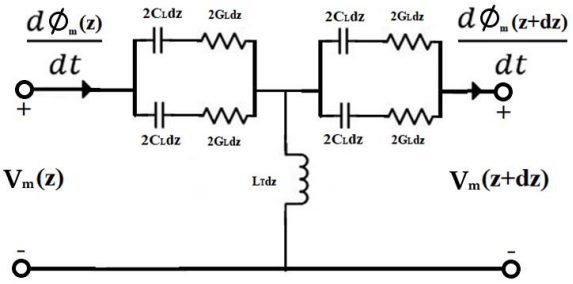

Figure 2: Magnetic transmission line circuit model.

This research attempts to present, for the first time, an extension of the novel magnetic transmission line model for modeling a saturated ferromagnet. This study discusses the effects of ferromagnetic resonance on the per unit length magnetic transmission line transverse impedance and longitudinal admittance. Using three-dimensional micro-magnetic finite difference time domain simulations, the precessional magnetization dynamics were analyzed. The broadband response of the magnetic transmission line was analyzed using pulse-perturbation technique. The amplitude, phase and ellipticity of the electromagnetic wave was used to calculate the propagation constant and wave impedance. Unwanted resonances due to reflections at boundary walls were avoided using perfectly matched boundary layers at the ends of the magnetic transmission line. The effect of complex permeability tensor elements and Gilbert damping constant on the propagation constant, intrinsic wave impedance, longitudinal magnetic admittance and transverse magnetic impedance were studied as well.

II. FDTD Electromagnetic Simulation

MIT Electromagnetic Equation Propagation (MEEP) software was used for the electromagnetic simulation of a gyromagnetic, dispersive, ferromagnetic transmission line. The finite difference time domain method discretizes Maxwell's equations using central difference approximations for space and time partial derivatives [16]. The different field components at a grid location are stored in the edges and faces of a cubic element called Yee's cell. The electromagnetic fields are evolved in discrete time steps $t_n = n\Delta t$ using leap frog method.

The dynamics of magnetic moments in magnetic materials is governed by the Landau Lifshitz Gilbert equation [9]:

$$\frac{d\boldsymbol{M}}{dt} = -\gamma\left(\boldsymbol{M} \times \boldsymbol{H_{eff}}\right) + \frac{\alpha\gamma}{M_s}\left(\boldsymbol{M} \times \frac{d\boldsymbol{M}}{dt}\right) \tag{6}$$

where $\boldsymbol{M}$ is the magnetization, γ is the gyromagnetic ratio, $\boldsymbol{H_{eff}}$ is the effective magnetic field, α is the phenomenological damping factor and M_s is the saturation magnetization. For a biased ferromagnet, the magnetization precesses around the bias field vector $\boldsymbol{b}$ according to Equation (7). It describes the Larmor precession of magnetic dipoles in response to an externally applied magnetic field. σ couples the magnetization to the driving field $\boldsymbol{H}$ and ω_0 is the angular frequency of precession. Only applied field contributions were considered for the effective magnetic field. Non-local effects like eddy currents,

long-range dipole-dipole interactions and exchange interactions between non-neighboring dipoles were not considered.

$$\frac{d\boldsymbol{M}}{dt} = -\boldsymbol{M} \times (\sigma \boldsymbol{H} + \omega_0 \boldsymbol{b}) + \frac{\alpha\gamma}{M_s}\left(\boldsymbol{M} \times \frac{d\boldsymbol{M}}{dt}\right) \quad (7)$$

Assuming that the magnetization $\boldsymbol{M}$ is a sum of static term $M\boldsymbol{b}$ parallel to the applied bias and a small perturbation term $\boldsymbol{m}$; the magnetization can be expressed as $\boldsymbol{M} = M\boldsymbol{b} + \boldsymbol{m}$. Hence, Equation (7) can be expressed as follows:

$$\frac{d\boldsymbol{m}}{dt} = -\sigma(M\boldsymbol{b} + \boldsymbol{m}) \times \boldsymbol{H} - \omega_0 \boldsymbol{m} \times \boldsymbol{b} + \frac{\alpha\gamma}{M_s}(M\boldsymbol{b} + \boldsymbol{m}) \times \frac{d\boldsymbol{m}}{dt} \quad (8)$$

Equation (8) is solved in MEEP using midpoint discretization method [16] to determine the magnetization $\boldsymbol{M}$ at every point on the Yee's grid. Assuming both $\boldsymbol{m}$ and $\boldsymbol{H}$ have harmonic time dependence $e^{-i\omega t}$, Equation (8) can be simplified to

$$-i\omega\boldsymbol{m} = \boldsymbol{b} \times \left(-\sigma M\boldsymbol{H} + \omega_0 \boldsymbol{m} - i\omega\frac{\alpha\gamma M}{M_s}\boldsymbol{m}\right) - \sigma \boldsymbol{m} \times \boldsymbol{H} \quad (9)$$

For ferromagnetic media biased in the z-direction, $\boldsymbol{b} = 1\boldsymbol{z}$. Hence, the solution of Equation (9) is

$$\boldsymbol{m} = [\chi]\boldsymbol{H} = \begin{bmatrix} \chi_{11} & -j\chi_{12} & 0 \\ j\chi_{21} & \chi_{22} & 0 \\ 0 & 0 & \chi_{33} \end{bmatrix} \quad (10)$$

where $\chi_{11} = \chi_{22} = \frac{\sigma M(\omega_0 - i\omega\kappa)}{(\omega_0 - i\omega\kappa)^2 - \omega^2}$, $\chi_{12} = \chi_{21} = \frac{\sigma M\omega}{(\omega_0 - i\omega\kappa)^2 - \omega^2}$, $\chi_{33} = 0$ and $\kappa = \frac{\alpha\gamma M}{M_s}$.

Equation (10) implies that the susceptibility tensor has skew-symmetric off-diagonal entries. When a plane wave that is linearly polarized along x-axis is launched in the z-direction, the polarization vector precesses around the z-axis as the wave propagates. Hence, the magnetization executes a damped counterclockwise rotation around the bias vector $\boldsymbol{b}$. Ferromagnetic resonance is observed when the angular frequency of the applied field matches the angular frequency of precession ω_0.

The Maxwell curl equations can be expressed in the frequency domain [10] as

$$\nabla \times \boldsymbol{E} = -i\omega[\mu]\boldsymbol{H} \quad (11)$$

$$\nabla \times \boldsymbol{H} = i\omega[\varepsilon]\boldsymbol{E} \quad (12)$$

where $[\mu]$ is the magnetic permeability tensor and $[\varepsilon]$ is the electric permittivity tensor. The H_x and H_y fields are coupled due to the off-diagonal terms in the susceptibility tensor (10). The resulting equations for the evolution of magnetic field components are:

$$B_x(\vec{r}) = \mu_0[1 + \chi_{11}(\vec{r}, \omega)]H_x(\vec{r}) - j\mu_0\chi_{12}(\vec{r}, \omega)H_y(\vec{r}) \quad (13)$$

$$B_y(\vec{r}) = \mu_0[1 + \chi_{22}(\vec{r}, \omega)]H_y(\vec{r}) + j\mu_0\chi_{21}(\vec{r}, \omega)H_x(\vec{r}) \quad (14)$$

$$B_z(\vec{r}) = \mu_0[1 + \chi_{33}(\vec{r}, \omega)]H_z(\vec{r}) \quad (15)$$

Equations (13) – (15) are solved in MEEP by taking the inverse Fourier transform and discretizing the resulting equations [13]:

$$B_x(\vec{r}, n\Delta t) = \mu_0 \left[H_x(\vec{r}, n\Delta t) + \int_0^{n\Delta t} H_x(\vec{r}, n\Delta t - \tau)\chi_{11}(\vec{r}, \tau)\, d\tau - \int_0^{n\Delta t} H_y(\vec{r}, n\Delta t - \tau)\chi_{12}(\vec{r}, \tau)\, d\tau\right] \quad (16)$$

$$B_y(\vec{r}, n\Delta t) = \mu_0 \left[H_y(\vec{r}, n\Delta t) + \int_0^{n\Delta t} H_y(\vec{r}, n\Delta t - \tau)\chi_{22}(\vec{r}, \tau)\, d\tau + \int_0^{n\Delta t} H_x(\vec{r}, n\Delta t - \tau)\chi_{21}(\vec{r}, \tau)\, d\tau\right] \quad (17)$$

$$B_z(\vec{r}, n\Delta t) = \mu_0 \left[H_z(\vec{r}, n\Delta t) + \int_0^{n\Delta t} H_z(\vec{r}, n\Delta t - \tau)\chi_{33}(\vec{r}, \tau)\, d\tau\right] \quad (18)$$

Finite difference time domain simulator MEEP solves these equations by the modified Yee's algorithm. The continuous integrals in (16) - (18) were implemented using discrete sums [16].

III. Simulation Results

Time dependent micromagnetic simulations were carried out in MEEP to understand the dynamics of ferromagnetic resonance. The sample permalloy ferromagnet used for the simulation had the following parameters: gyromagnetic ratio $\gamma = 2\pi \times 23.8$ GHz/T, saturation magnetization $M_s = 790\ kA/m$, Gilbert

damping constant $\alpha = 10^{-5} - 10^{-2}$ and relative permittivity ε_r = 1.5 [9]. The frequency dependent nature of the non-diagonal susceptibility element χ_{12} is shown in Figure 3. For a high quality crystal oscillator, the resonance has a very large peak due to the small Gilbert damping factor α. The magnetic susceptibility was enforced; hence the impedance and transmission characteristics of the transmission line were pre-determined since the resonance frequency and permeability were set.

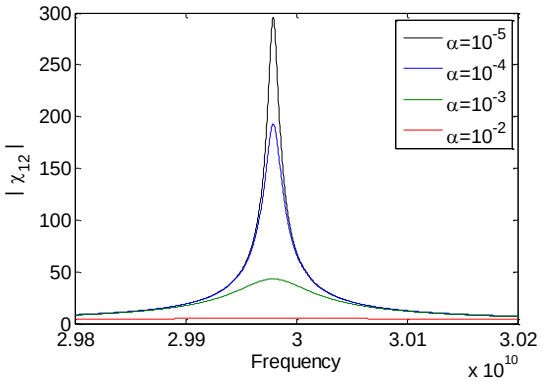

Figure 3: Ferromagnetic resonance of susceptibility tensor element χ_{12}.

The geometry of the micromagnetic simulation setup is shown in Figure 4. The grid was divided into a 3-D array of cubic cells with the dimensions 10nm × 10 nm × 10nm. The ferromagnetic sample had the dimensions 40nm × 40nm × 23μm. The time step was chosen as $\Delta t = (1/60)$fs. A perfectly matched boundary layer with 1600 cells was added on both ends of the transmission line. The perfectly matched boundary layer had a width of 1μm. The bias magnetic field was applied in z-direction and it had a magnitude of 1000 kA/m. The angular frequency of precession was ω_0 = 2π×30-GHz. Tangential and normal components of the magnetic field were continuous on the boundaries of the magnetic structure.

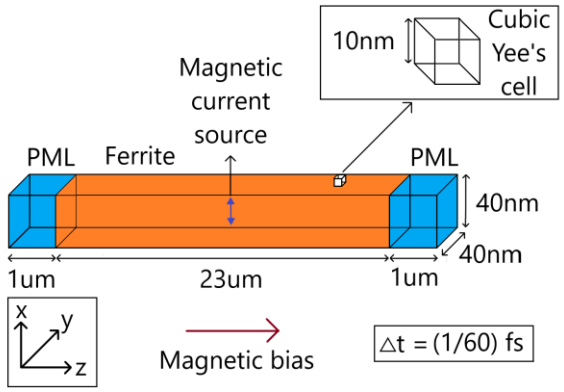

Figure 4: Geometry of micromagnetic simulation setup in MEEP. The diagram is not drawn to scale.

A Gaussian soft magnetic current source (oscillating magnetic dipole) $I_m(t)$ was placed in the magnetized ferrite. The Fourier transform of the source is plotted in Figure 5. The source launched a z-directed wave which was linearly polarized in x-direction. As the magnetic field propagated through the magnetized ferrite, the resultant polarization changed continuously as the different frequency components experienced different rates of rotation per unit distance of propagation. Hence, the magnetic field was heavily deformed as it reached the output end.

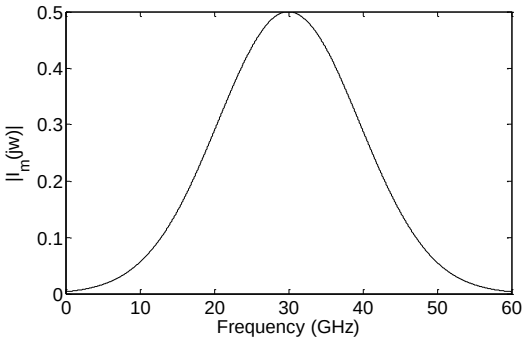

Figure 5: Fourier transform of the applied magnetic current source $|I_m(j\omega)|$ plotted for the frequency range 0-60 GHz.

The 30-GHz harmonic of the incident wave matched the Larmor frequency and gave rise to gyromagnetic resonance. The Gilbert damping constant was varied to simulate the effect of magnetic hardness on the ferromagnetic resonance. Gilbert damping constant depends on the crystal structure, chemical composition, ferrite grain size, structural dimensions and annealing temperature [5]. A high quality crystal oscillator must have a very low Gilbert damping constant, so that it can absorb millimeter waves efficiently [11].

The wave impedance shown in Figure 6 was calculated using the Fourier transform of a small window of input and output signals, during steady state of gyromagnetic resonance. The intrinsic wave impedance spikes due to the high magnetic susceptibility and magnetic permeability during the 30-GHz gyromagnetic resonance. The value of intrinsic wave impedance increases the electromagnetic power losses across the ferrite. It absorbs a lot of electromagnetic energy from the transverse field and starts to heat up. The intrinsic wave impedance dropped when the Gilbert damping constant was increased.

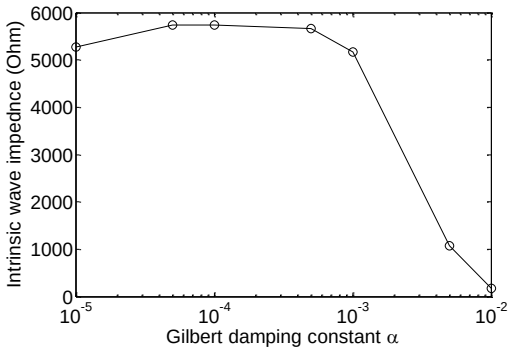

Figure 6: Plot of intrinsic wave impedance calculated at 30-GHz vs. Gilbert damping constant.

The phase constant and attenuation constant were calculated for the resultant electromagnetic wave. The calculated wave attenuation constant is shown in Figure 7, which was calculated by comparing the magnetic field strength at input and output sides. The output signal was heavily attenuated compared to the input signal hence the attenuation constant was very high during the 30-GHz gyromagnetic resonance. A high quality crystal oscillator, with a small Gilbert damping constant, showed a strong peak of the electromagnetic absorption spectrum. When the Gilbert damping constant was increased, the attenuation constant and the electromagnetic absorption decreased.

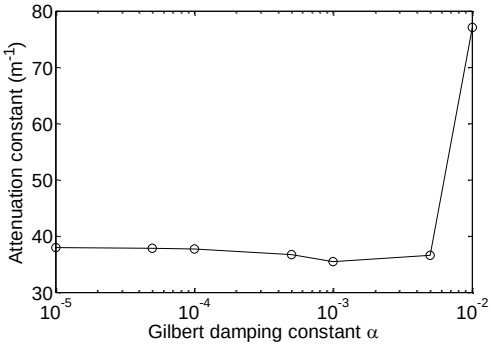

Figure 7: Plot of attenuation constant calculated at 30-GHz vs. Gilbert damping constant.

The magnetic susceptibility was enforced; hence the impedance and transmission characteristics of the transmission line were pre-determined since the resonance frequency and permeability were set. After calculating the propagation constant and intrinsic wave impedance, the magnetic transmission line longitudinal admittance and transverse impedance were calculated using (4) – (5).

The calculated per unit length longitudinal admittance during 30-GHz gyromagnetic resonance is shown in Figure 8. Ferromagnetic resonance leads to a severe increase in power dissipation in the ferrite sample which makes the ferrite sample highly conductive to electromagnetic flux. The ferromagnetic sample absorbs a lot of electromagnetic energy and starts to heat up. The complex permittivity and magnetic permeability dictate the dielectric and magnetic losses of the resonating sample. When the Gilbert damping constant was increased, the longitudinal magnetic admittance increased as well.

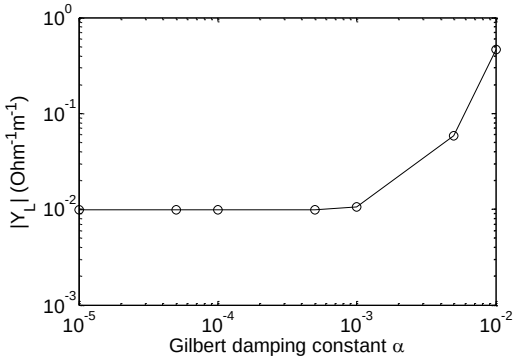

Figure 8: Plot of longitudinal magnetic admittance calculated at 30-GHz vs. Gilbert damping constant.

The calculated per unit length transverse magnetic impedance during 30-GHz gyromagnetic resonance is shown in Figure 9. The resonance of Larmor precession leads to a severe increase in power dissipation in the ferrite sample. The magnetic flux leakage drops heavily and this makes the ferrite sample highly conductive to electromagnetic flux. Ultimately, the ferrite sample absorbs a lot of electromagnetic energy. When the Gilbert damping constant was increased, the transverse magnetic impedance dropped. This indicated an increase in the magnetic flux leakage across the magnetized ferrite.

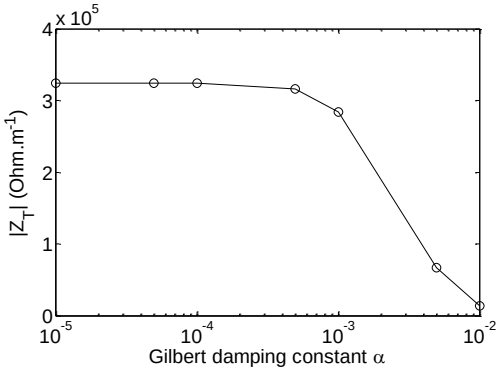

Figure 9: Plot of transverse magnetic impedance calculated at 30-GHz vs. Gilbert damping constant.

IV. Discussion

The non-linear and anisotropic nature of magnetized ferrites was modeled using linearized Landau Lifshitz Gilbert equation (8). The magnetic susceptibility tensor had skew-symmetric off-diagonal entries hence the magnetization exhibited damped precession around the gyrotropy axis [17]. The bias field produced Zeeman splitting in energy levels and the saturated magnetic dipoles transitioned between the energy levels by absorbing millimeter wave electromagnetic fields [9].

Finite difference micro-magnetic simulations accurately modeled the precessional magnetization dynamics. The frequency dependent complex dynamic susceptibility tensor determined the steady state amplitude, phase and ellipticity of the electromagnetic wave during millimeter wave ferromagnetic resonance. Unwanted resonances due to reflections at boundary walls were avoided using perfectly matched boundary layers at the ends of the magnetic transmission line [9]. The broadband response of the magnetic transmission line was analyzed using pulse-perturbation technique.

When the Gilbert damping constant was increased, the damping for precessional motion increased. From Figures 6 and 7, it can be deduced that this caused the intrinsic wave impedance to decrease and the attenuation constant to increase. Hence, the electromagnetic absorption of millimeter waves reduced significantly. The result can be explained using the off-diagonal entries in the magnetic susceptibility tensor (10). The magnitude of the off-diagonal entries decreases with Gilbert damping constant. Hence the effective magnetic susceptibility decreases.

The electromagnetic properties of the transmission medium were modeled using an equivalent transverse magnetic impedance and the longitudinal magnetic admittance shown in Figure 2. From the results of micromagnetic finite difference time domain simulations, the longitudinal magnetic admittance and transverse magnetic impedance were calculated using (4) - (5). The per unit length transverse magnetic inductance L_T represents a magnetic energy storage element; the per unit length longitudinal capacitance C_L represents an electric energy storage element; and the per unit length magnetic conductance G_L dissipates energy.

As shown in Figure 8, the longitudinal magnetic admittance $Y_L(j\omega) = G_L + j\omega C_L$ was small during ferromagnetic resonance. Hence, it provided a low reluctance path for magnetic flux. The nano-magnets exhibited a strong absorption of millimeter wave which resulted in a high attenuation constant. From Figure 9, it can be deduced that the magnetic flux leakage was low during ferromagnetic resonance because the transverse magnetic impedance $Z_T(j\omega) = j\omega L_T$ was very high.

When the Gilbert damping constant was increased, the effective magnetic susceptibility decreased. The magnetic reluctance increased and the absorption of electromagnetic energy was reduced. As shown in Figure 8, this resulted in an increase in the longitudinal magnetic admittance $Y_L(j\omega) = G_L + j\omega C_L$. Meanwhile, the magnetic flux leakage increased which resulted in the drop of transverse magnetic impedance $Z_T(j\omega) = j\omega L_T$ in Figure 9.

The intrinsic wave impedance and attenuation constant were strong functions of effective magnetic susceptibility [7]. The drop in longitudinal admittance and the increase in transverse impedance explains the high electromagnetic power losses during resonance of Larmor precession. For a high quality crystal with a small Gilbert damping constant, the effect is seen clearly in Figures 8 and 9. The saturated ferrite absorbs electromagnetic energy from the input microwave signal and heats up. If the Gilbert damping constant is increased, the effect is less pronounced. This is because the effective magnetic susceptibility increases slightly during ferromagnetic resonance, and the Larmor precession is highly damped.

V. Conclusion

A magnetic transmission model was presented for a saturated ferrite exhibiting ferromagnetic resonance. Finite difference time domain simulation was used to study the effects of gyromagnetic resonance on its longitudinal magnetic admittance and transverse magnetic impedance. The gyromagnetic precession of saturated magnetic dipoles was accurately modeled using linearized Landau-Lifshitz-Gilbert model in MEEP simulator. It was shown that ferromagnetic resonance leads to a drastic increase in the transverse magnetic impedance and the electromagnetic energy losses of longitudinal magnetic admittance. The quality of the crystal oscillator is dictated by Gilbert damping constant. When the precessional damping was increased, the electromagnetic absorption of millimeter waves was reduced due to the high longitudinal magnetic admittance and low transverse magnetic impedance. These results are useful for modern high frequency applications of gyromagnetic materials like spintronic devices, space navigation, wireless communication, maritime and geophysical prospecting instruments.

REFERENCES

[1] R. Bowrothu, H. Kim, C. Smith, D. Arnold and Y. Yoon, "35-GHz Barium Hexaferrite/ PDMS composite-based millimeter-wave circulators for 5G applications", *IEEE Transactions on Microwave Theory and Techniques*, Vol. 68, No. 12, pp. 5065-5071, 2020.

[2] K. Alhassoon, Y. Malallah and A. Daryoush, "Complex permittivity and permeability extraction of ferromagnetic materials for magnetically tuned microwave circuits", *IEEE Journal of Microwaves*, Vol. 1, No. 2, pp. 639-645, 2021.

[3] L. Chao, A. Sharma and M. N. Afsar, "Microwave and millimeter wave ferromagnetic absorption of nanoferrites", *IEEE Transactions on Magnetics*, Vol. 48, No. 11, pp. 2773–2776, 2012.

[4] J. Xu, M. Koledintseva, Y. Zhang, Y. He, B. Matlin, R. Dubroff, J. Drewniak and J. Zhang, "Complex permittivity and permeability measurements and finite-difference time-domain simulation of ferrite materials", *IEEE Transactions on Electromagnetic Compatibility*, Vol. 52, No. 4, pp. 878-887, 2010.

[5] T. Ovari, H. Chiriac, M. Vazquez and A. Hernando, "Correlation between the magneto-impedance and ferromagnetic resonance responses in nanocrystalline microwires", *IEEE Transactions on Magnetics*, Vol. 36, No. 5, pp. 3445-3447, 2000.

[6] N. Adachi, D. Uematsu, T. Ota, M. Takahashi, K. Ishiyama, K. Kawasaki, H. Ota, K. Arai, S. Fujisawa, S. Okubo and H. Ohta, "Far-infrared ferromagnetic resonance of magnetic garnet for high frequency electromagnetic sensor", *IEEE Transactions on Magnetics*, Vol. 46, No. 6, pp. 1986–1989, 2010.

[7] K. Coakley, P. Kabos and S. Johnson, "Determination of effective magnetization and gyromagnetic ratio of Yttrium Iron garnet from multi-mode ferromagnetic resonance S21 spectra", *IEEE Transactions on Magnetics*, Vol. 57, No. 5, 6100706, pp. 1-6, 2021.

[8] Y. Zhang, J. Um, B. Stadler and R. Franklin, "Permeability and ferromagnetic resonance study for magnetic nanowires substrate with Copper layer", *IEEE Microwave and Wireless Components Letters*, Vol. 30, No. 11, pp. 1065-1068, 2020.

[9] K. Wagner, L. Korber, S. Stienen, J. Lindner, M. Farle and A. Kakay, "Numerical ferromagnetic resonance experiments in nanosized elements", *IEEE Magnetics Letters*, Vol. 12, 6100205, pp. 1-5, 2021.

[10] H. Al-Barqawi, N. Dib and M. Khodier, "A full-wave two-dimensional finite-difference frequency-domain analysis of ferrite-loaded structures", Mosharaka International Conference on Communications, Propagation and Electronics, Vol. 29, pp. 1-6, 2008.

[11] D. Ozaki, D. Miura and A. Sakuma, "Theoretical study of Gilbert damping constants in magnetic multilayer films", *IEEE Transactions on Magnetics*, Vol. 55, No. 7, 1300505, pp. 1-5, 2019.

[12] M. Rajaram, A. Rajamani, P. Muthuraj, B. Arumugam and K. Natarajan, "Investigation of left-handed behavior in ferromagnetic Cobalt magnetic vortex structure using spin-wave resonances", *IEEE Transactions on Magnetics*, Vol. 56, No. 8, 1300210, pp. 1-10, 2020.

[13] A. Taflove and S. Hagness, *Computational electrodynamics: the finite-difference time-domain method*, Third Edition, Boston: Artech House, pp. 237-245, 2005.

[14] J. Faria and M. Pires, "Theory of magnetic transmission lines", *IEEE Transactions on Microwave Theory and Techniques*, Vol. 60, No. 10, pp. 2941–2949, 2012.

[15] J. Faria, "Formulation of multiwire magnetic transmission-line theory", *Progress in Electromagnetics Research B*, Vol. 49, pp. 177-195, 2013.

[16] A. Oskooi, D. Roundy, M. Ibanescu, P. Bermel, J. Joannopoulos and S. Johnson, "MEEP: a flexible free-software package for electromagnetic simulations by the FDTD method", *Computer Physics Communications*, Vol. 181, pp. 687-702, 2010.

[17] D. Seddaoui, S. Loranger, M. Malatek, D. Menard and A. Yelon, "The nonlinear Landau-Lifshitz equation: ferromagnetic resonance, giant magnetoimpedance, and related effects", *IEEE Transactions on Magnetics*, Vol. 47, No. 2, pp. 279-283, 2011.